PCCP

View Online
Dynamic Article Links

Cite this: *Phys. Chem. Chem. Phys.*, 2011, **13**, 818–824

www.rsc.org/pccp

PAPER

Chiral recognition between 1-(4-fluorophenyl)ethanol and 2-butanol: higher binding energy of homochiral complexes in the gas phase†

Flaminia Rondino,[ab] Alessandra Paladini,[c] Alessandra Ciavardini,[a] Annarita Casavola,[c] Daniele Catone,[d] Mauro Satta,[e] Hans Dieter Barth,[f] Anna Giardini,[c] Maurizio Speranza[b] and Susanna Piccirillo*[a]

Received 2nd August 2010, Accepted 11th November 2010
DOI: 10.1039/c0cp01401j

Diastereomeric adducts between (*S*)-1-(4-fluorophenyl)-ethanol and *R* and *S* 2-butanol, formed by supersonic expansion, have been investigated by means of a combination of mass selected resonant two-photon ionization-spectroscopy and infrared depletion spectroscopy. Chiral recognition is evidenced by the specific spectroscopic signatures of the $S_1 \leftarrow S_0$ electronic transition as well as different frequencies and intensities of the OH stretch vibrational mode in the ground state. D-DFT calculations have been performed to assist in the analysis of the spectra and the determination of the structures. The homochiral and heterochiral complexes show slight structural differences, in particular in the interaction of the alkyl groups of 2-butanol with the aromatic ring. The experimental results show that the homochiral [$FE_S{\cdot}B_S$] complex is more stable than the heterochiral [$FE_S{\cdot}B_R$] diastereomer in both the ground and excited states. The binding energy difference has been evaluated to be greater than 0.60 kcal mol^{-1}.

1. Introduction

It is wholly accepted that aggregation and self-recognition played an important role in the prebiotic earth.[1] Over the several hundred million years of chemical evolution that brought to the first living organisms, simple molecules evolved into larger and more complex systems, often through processes mediated by supramolecular interactions. Chirality is an important element of terrestrial life: life as we know it cannot possibly function without chirality either at the molecular or the supramolecular level. Various hypotheses have been proposed to explain the abiotic origin of chirality.[2] However, several evolutionary steps were required to produce, implement, and maintain chirality in the terrestrial type of life.[3] The specific chemical mechanisms that lead to the first replicable homochiral substance still remain unknown, though it is certain that chiral recognition through supramolecular interactions played a major role in the prebiotic earth and in the evolution of life. The in-depth comprehension of stereospecific, non-covalent interactions is a major issue to understand the origin of life and all processes that occur in living organisms.

Information on molecular structure, dynamics, reactivity, energetics of diastereomeric complexes can be achieved by spectroscopic techniques. One may broadly distinguish between spectroscopic techniques operating with samples in the condensed phases[4–6] (in liquids, on surfaces, and in structured materials), which are the majority, and experiments in the gas phase (on isolated complexes). Though it can be argued that the properties of isolated complexes cannot be directly extended to the condensed phase, gas phase studies have the advantage that tailor-made diastereomeric clusters can be investigated at the molecular level and are appropriate for an accurate understanding of the forces at play in chiral recognition. Fundamental interactions, influencing specific molecular geometries,[7] as well as the dynamics of conceivable reactive processes can be studied without any interference from the environment. The results of gas phase experiments can be used by theoretical chemists as a benchmark for the validation of different approximations for *ab initio* calculations.

In this context, several groups, including ours, have been active in investigating weakly bound diastereomeric clusters. To elucidate the nature of the intervening intracomplex forces and the underlying mechanisms it is desirable to investigate small model systems which can be generated and isolated by supersonic expansion. Hydrogen bonded clusters are of particular interest because of their ubiquitous role in biological systems. Their structure and conformational equilibria have been

[a] *Dip. di Scienze e Tecnologie Chimiche, Università di Roma "Tor Vergata", via della Ricerca Scientifica, 00133 Rome, Italy. E-mail: piccirillo@fisica.uniroma2.it*
[b] *Dip. di Chimica e Tecnologie del Farmaco, Università di Roma "La Sapienza", Rome, Italy*
[c] *CNR – IMIP, Tito Scalo (PZ), Italy*
[d] *CNR – ISM, Rome, Italy*
[e] *CNR – ISMN, Rome, Italy*
[f] *Institut für Physikalische und Theoretische Chemie, J. W. Goethe-Universität Frankfurt, Germany*

† Electronic supplementary information (ESI) available: B3LYP, D-B3LYP, B97D, WB97XD calculations results. See DOI: 10.1039/c0cp01401j

characterized by several spectroscopic methodologies, such as LIF (Laser Induced Fluorescence),[8] R2PI (Resonant Two Photon Ionization),[9] RET (Rydberg Electron Transfer),[10] FTIR (Fourier Transform Infrared)[11] and microwave spectroscopies.[12]

Resonant Two Photon Ionization (R2PI) spectroscopy, coupled with Time of Flight (TOF) mass spectrometry, is a powerful tool for studying non-covalent molecular interactions involved in chiral recognition. It provides mass-selective electronic spectra and allows the energetic and structural characterization of neutral diastereomeric complexes and the investigation of chemical reactivity in ion complexes.[13] An important aspect of R2PI studies concerns the measure of the binding energy differences in a few adducts between chiral benzylic alcohol derivatives and chiral secondary alcohols, which is in the range of 250–400 cm^{-1} with the homochiral complexes always more stable than the corresponding heterochiral complexes.[13,14] Recently we have applied this methodology to fluorinated analogues[15,16] of chiral aromatic alcohols, with the aim of determining the effect of fluorine substitution on the structure and reactivity properties of their complexes and to verify the role of the fluorine substitution on the chiral recognition process. Organofluorine compounds, although rare in nature, are increasingly applied in metabolic studies, in positron emission tomography, as antitumor agents, and as probes in studying enzyme activity, reaction mechanisms, and biomolecular binding.[17]

In this paper, we report on the application of R2PI-TOF spectroscopy and IR-R2PI double resonance spectroscopy to gas phase diastereomeric complexes of a chiral chromophore *e.g.* (*S*)-1-(4-fluorophenyl)-ethanol (FE_S) with *R*-2-butanol and *S*-2-butanol ($B_{R/S}$). Because of the stereospecificity of the chromophore–solvent interaction, the corresponding hetero [FE_S·B_R] and homochiral [FE_S·B_S] diastereomeric pairs display specific spectroscopic signatures, namely, the electronic band origin of each pair, their vibronic bands and their dissociation thresholds. IR-R2PI double resonance experiments allowed us to measure the ground state O–H stretching frequencies of [FE_S·B_S] and [FE_S·B_R] and to check the presence of different ground-state isomers. The results have been interpreted with the aid of theoretical predictions at the D-B3LYP level of theory.

2. Experimental and computational methodology

2.1 Experimental section

The molecular beam chamber combined with the linear time of flight (TOF) mass spectrometer used in this work has been previously described[18] and only a brief account will be given here. Diastereomeric clusters were generated in a supersonic-jet expansion of a carrier gas (Ar; stagnation pressure 2 bar) seeded with FE_S, and B_R or B_S, through a heated (80 °C) pulsed valve (0.8 mm id, aperture time: 200 μs). The concentration is maintained low enough to minimise the production of heavier clusters.

The supersonic jet was skimmed before entering the detection chamber. At a distance of about 13 cm from the nozzle the clusters are ionized in the ionization region of a time of flight mass spectrometer *via* one color R2PI (1cR2PI) utilizing a Nd:YAG-pumped pulsed dye laser with associated crystals for nonlinear optical conversion. The laser beam is perpendicular to the supersonic beam. The photoions are mass analyzed and detected by a channeltron. The signal was recorded and averaged by a digital oscilloscope and stored on a PC.

The 1cR2PI experiments involve electronic excitation of the species of interest by absorption of one photon $h\nu_1$ at resonance with an electronic transition of the cluster and by its ionisation by a second photon of the same energy $h\nu_1$. The 1cR2PI excitation spectra were obtained by recording the ion yield as a function of ν_1. Due to the resonant step in the two-photon ionization, the 1cR2PI spectrum reflects the UV excitation spectrum of the neutral precursor.

By fixing the UV ionization laser to one of the cluster-specific transitions in its 1cR2PI spectrum, the vibrational spectra in the OH-stretching region of the neutral precursors have been recorded by IR-R2PI double-resonance spectroscopy. The IR and UV lasers are counterpropagating and spatially superimposed; the IR pulse (pump) precedes the UV laser pulse (probe) by about 100 ns. If the IR laser is at resonance with vibrational transitions of the ground state of the cluster, the ground state population is depleted and the cluster can predissociate by absorption of one or several energy quanta. This results in a reduction of the number of ions produced by 1cR2PI. By measuring the ion signal while tuning the IR wavelength, the so called IR-R2PI depletion spectrum represents the vibrational transitions of the neutral precursor in the S_0 ground state. This methodology also allows the discrimination of different stable conformations present in the supersonic molecular beam.[19] Several factors can affect the conformer distribution following supersonic expansion. For isolated molecules, the Boltzmann conformer distribution before the expansion may be preserved provided that interconversion barriers between conformers are sufficiently high. The collisional relaxation during the free jet expansion, on the other hand, may partly drain the population into the most stable conformational structures. This is also true for clusters, which are formed and stabilized during the free jet expansion. The distinction of conformers by IR-R2PI is achieved by selecting the frequency of the UV laser. UV absorption frequencies pertaining to different conformers will display a different IR spectrum.

The IR laser light is generated by a recently homemade, injection-seeded optical parametric oscillator (OPO), which has been built according to the design developed at the University of Frankfurt.[20] The seed optical signal around 3 μm is produced by mixing, in a $LiNbO_3$ crystal, 10 mJ at 532 nm (Brilliant B Nd:YAG laser) with 3 mJ at 640–670 nm, produced by a tunable dye laser pumped by the same YAG laser second harmonic. 100–200 μJ of IR light is obtained and it is used to inject an OPO laser cavity. The OPO utilizes another $LiNbO_3$ crystal and is pumped by 110 mJ of a 1064 nm laser beam, still from the same Brilliant B YAG laser. Typical idler output (2.6–3.7 μm) energies are about 2–3 mJ per pulse. The tunable range with a DCM dye in DMSO covers the 3000–3900 cm^{-1} region with a bandwidth of 0.8 cm^{-1}, except for a dip in between 3487 and 3510 cm^{-1} that is due to OH impurities in the $LiNbO_3$ crystals. The FE_S, B_R and B_S samples were purchased from Sigma Aldrich and used without further purification.

2.2 Theoretical section

Because of the complexity of the potential energy surfaces of the [$FE_S \cdot B_{S/R}$] clusters a preliminary search of the energy minima has been performed by restrained molecular dynamics calculations using the Tinker Package.[21] In particular the MM3[22] force field has been used to run molecular dynamics at a temperature of 800 K with constrain to overcome dissociation (cumulative time of 0.1 ns, dump time 1 ps). 100 snapshots are then optimized with a convergence of 10^{-6} kcal mol^{-1} $Å^{-1}$ RMS gradient per atom. The optimized structures are then classified according to their topology. Six lowest energy structures for each diastereomer ($E < 2$ kcal mol^{-1}) have been re-optimized using *ab initio* procedures. Because the strong hydrogen bond contribution to the intermolecular forces is almost similar for the various conformers, the energy differences of these molecular systems are substantially affected by weak dispersive interactions. Therefore a detailed and comparative study has been carried out by employing different approximated hamiltonians within the density functional theory. In particular B3LYP (with and without dispersive contribution), B97D and WB97XD functionals[23] have been used in order to estimate the vibrational frequencies. The *ab initio* calculations have been performed with 6-31++G** basis set. The frequency analysis has been based on normal mode harmonic approximation, and a scaling factor of 0.9613 has been used.[24] All the above *ab initio* calculations have been executed with Gaussian03,[25] NWCHEM,[26] and GAMESS-US[27] program packages.

3. Results and discussion

3.1 Electronic and vibrational spectroscopy: 1cR2PI and IR-R2PI spectra

One color R2PI spectroscopy is able to discriminate between homochiral and heterochiral complexes through the measure of their excitation spectra and of the specific spectral shifts with respect to that of the bare chromophore. Because of the low internal temperature of the species present in the supersonic beam, the spectra display well-resolved features since only the lowest rotational and vibrational levels of the electronic ground states are populated. Through IR-R2PI double resonance experiments the O–H stretching frequencies of B_R and B_S bound to FE_S have been measured.

Fig. 1 reports the 1cR2PI excitation spectra of the two [$FE_S \cdot B_S$] and [$FE_S \cdot B_R$] diastereomeric complexes recorded with pure enantiomers in the 36 800–37 900 cm^{-1} frequency range. A spectral chiral discrimination is evident from the spectra: each diastereomer displays distinct features shifted to the red with respect to 0_0^0 transition of the chromophore (dotted line in Fig. 1).[16]

The spectrum of the homochiral [$FE_S \cdot B_S$] complex is characterized by an intense band at 36 853 cm^{-1}, accompanied by a low frequency mode progression with a spacing of 17 cm^{-1} (bands labeled 1–7 in Fig. 1a and 5a). A similar band progression is observed in the 37 600–37 800 cm^{-1} ring breathing region of the spectrum (bands 11–14) (Table 1). As previously reported for FE_S and [$FE_S \cdot H_2O$],[16] the band progression is ascribable to the fact that the $S_1 \leftarrow S_0$ transition in these

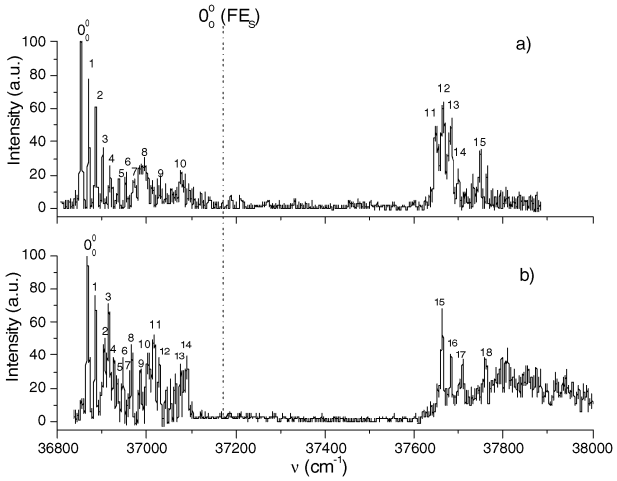

Fig. 1 1cR2PI excitation spectra of (a) homochiral [$FE_S \cdot B_S$] and (b) heterochiral [$FE_S \cdot B_R$] clusters, obtained by monitoring the ion signal at $m/z = 214$. The dotted line refers to the 0_0^0 electronic transition of the isolated FE_S molecule at 37 140 cm^{-1}.

Table 1 Experimental vibronic bands of the S_1 excited state of Fig. 1a, compared with the D-B3LYP/6-31G** calculated vibrational frequencies for the S_0 ground state of the A_{homo} conformer of the [$FE_S \cdot B_S$] cluster

Peak	Vibrational mode	ν_{th}/cm^{-1}	ν_{exp}/cm^{-1}	Mode description
1	ν_1	23	17	C_1–$C_\alpha$tors. + interm. bending
2	$2\nu_1$		33	"
3	$3\nu_1$		48	"
4	$4\nu_1$		65	"
5	$5\nu_1$		84	"
6	$6\nu_1$		101	"
7	$7\nu_1$		119	"
8	ν_2	131	143	Symmetric ring tors.
9	ν_3	162	163	C_2–C_3 butanol torsion
10	ν_4	230	224	Butanol CH_3 torsion + asym. ring tors.
11	ν_{33}	797	796	Asymm. butterfly
12	$\nu_{33} + \nu_1$		811	Asymm. butterfly + C_1–C_α tors. + interm. bend.
13	$\nu_{33} + 2\nu_1$		830	"
14	$\nu_{33} + 3\nu_1$		847	"
15	ν_{36}	871	896	Methyl bending

fluorinated species involves asymmetric structures of the aromatic ring in both the S_0 and S_1 states.

The spectrum of the heterochiral [$FE_S \cdot B_R$] complex exhibits two band progressions, the first starting at 36 867 cm^{-1} (bands 1, 2, 4 in Fig. 1b and 5b) and a less intense second one at 36 914 cm^{-1} (bands 3, 5, 7 in Fig. 1b and 5b), both characterized by the same spacing of 19 cm^{-1}. A similar band progression is also observed in the 37 600–38 000 cm^{-1} region of the spectrum.

The shifts of the 0_0^0 $S_1 \leftarrow S_0$ electronic transition of the diastereomeric complexes relative to the 0_0^0 electronic origin of the isolated FE_S are $\Delta\nu_{homo} = -287$ cm^{-1} and $\Delta\nu_{hetero} = -273$ cm^{-1}. A red shift indicates an enhancement of the binding energy for the clusters in the S_1 state relative to the S_0 state.

The $S_1 \leftarrow S_0$ energy gap is higher than what was observed for similar non-fluorinated systems, namely the complexes of

1-phenylethan-1-ol ($\Delta\nu_{homo}$ = −121 cm^{-1}, $\Delta\nu_{hetero}$ = −132 cm^{-1}),[14,28] 1-phenylpropan-1-ol ($\Delta\nu_{homo}$ = −79 cm^{-1}, $\Delta\nu_{hetero}$ = −92 cm^{-1})[13] and 2-naphthylethan-1-ol ($\Delta\nu_{homo}$ = −125 cm^{-1}, $\Delta\nu_{hetero}$ = −136 cm^{-1}),[29] with $B_{R/S}$.

The higher value of the spectral shift in [FE_S·$B_{R/S}$] with respect to non-fluorinated analogues can be attributed to the electron-withdrawing effect of the fluorine atom with respect to the aromatic ring, which is stronger in the excited π* state than in the π ground state, due to the higher polarizability of the aromatic ring in the excited state. A tentative explanation for the increase of the binding energy in the excited state could be that the decreased electron density on the aromatic ring determines a reduced repulsive solvent–chromophore electronic term.

Dispersive interactions between the aliphatic chain of the alcohol and the π-system of the chromophore are mainly responsible for the different spectral shifts observed in [FE_S·$B_{R/S}$] and in non-fluorinated analogues.

Fig. 2 reports the IR-R2PI depletion spectra of [FE_S·B_R] and [FE_S·B_S] complexes recorded in the 3500–3700 cm^{-1} range. The UV probe wavelength was set on the origin of the homochiral [FE_S·B_S] (36 853 cm^{-1}, band 0_0^0 in Fig. 1a) and heterochiral [FE_S·B_R] (36 867 cm^{-1}, band 0_0^0 in Fig. 1b) complex transition. One vibrational transition has been observed at 3637 cm^{-1} for [FE_S·B_S] and at 3610 cm^{-1} for [FE_S·B_R] with different intensities. Since the band at 36 914 cm^{-1} in the electronic spectrum of [FE_S·B_R] (band 3 in Fig. 1b) could be interpreted as being due to the 0_0^0 electronic transition of the another isomer we probed the depletion also on this band. We found that it yields an IR-R2PI depletion signal at exactly the same frequency as with band 0_0^0 with comparable efficiency, and thus the two bands may be attributed to one common precursor.

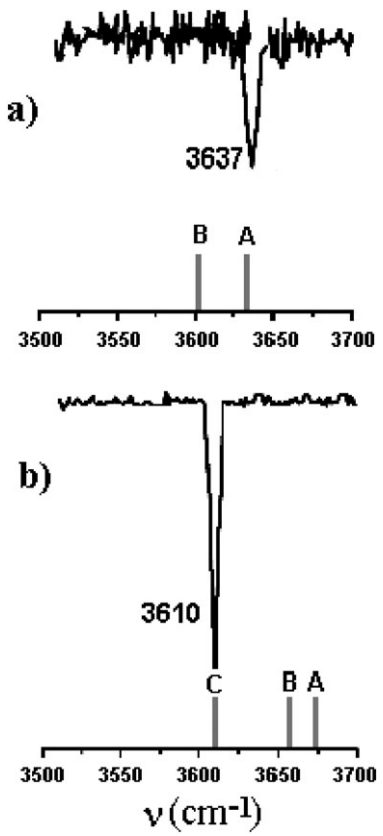

Fig. 2 IR-R2PI spectrum of (a) [FE_S·B_S] probe set at 36 853 cm^{-1} and (b) [FE_S·B_R] probe set at 36 867 cm^{-1}. D-B3LYP/6-31G** calculated vibrational frequencies for the S_0 ground state are reported with gray bars.

The bands at 3637 and 3610 cm^{-1} correspond to the OH stretch mode of butanol in the [FE_S·$B_{R/S}$] clusters (νO^bH). The lower value of the νO^bH stretching frequency measured for the [FE_S·B_R] as compared to [FE_S·B_S] indicates that the hydrogen bond interaction at play in the [FE_S·B_R] complex should be slightly stronger.

3.2 Mass spectra, dissociation thresholds and binding energy differences

In a 1cR2PI process, if the excited state is much higher in energy than one-half of the ionization energy, the ion will be produced with a not negligible excess energy which results in vibrational excitation of the ionized species. Sometimes, this excitation causes the cluster ion to dissociate into its original components or give rise to more complex fragmentation patterns.[13,15,30] The dissociation ratio in the 1cR2PI process of non-covalent diastereomeric complexes provides a further tool for their discrimination. A great difference in the dissociation ratios in correspondence with small differences in the total energy ($2h\nu_1$) absorbed in the process indicates that higher-energy dissociative states are populated in the cluster that shows the higher dissociation ratio.

[FE_S·$B_{R/S}$] complexes are a favourable case in which the difference in the binding energies can be evaluated in a 1cR2PI experiment. This is because the excited state energy is almost half way between the ground electronic state and the dissociation threshold of the cluster.

The 1cR2PI mass spectra of a mixture of FE_S and $B_{R/S}$ recorded in correspondence with the 0_0^0 $S_1 \leftarrow S_0$ origin transitions are shown in Fig. 4a and b. They are characterized by the predominance of the [FE_S·$B_{R/S}$]$^+$ molecular ion at m/z = 214. Only for [FE_S·B_R]$^+$ a certain amount of the dissociation fragment [FE_S]$^+$ at m/z = 140 is present. The overall energy ($E_{2h\nu}$) imparted to the relevant neutral [FE_S·$B_{R/S}$] complexes in the 1cR2PI experiments at the origin transitions wavelength is 73 706 cm^{-1} for [FE_S·B_S] and 73 734 cm^{-1} for [FE_S·B_R]. The presence in the mass spectrum of [FE_S]$^+$ indicates that for the heterochiral complex, $E_{2h\nu}$ is higher than the dissociation threshold of the ionic adduct.

Fig. 4c and d show the mass spectra recorded in correspondence with the vibronic transitions labelled 11 in Fig. 1a and 15 in Fig. 1b. The fragmentation ratio $I_{[FE_S]+}/I_{[FE_S]+} + I_{[FE_S\ B_{S/R}]+}$ in the 1cR2PI process at these wavelengths is 51% for the [FE_S·B_S] complex and 88% for the [FE_S·B_R] complex. In this case the overall energy imparted to the relevant neutral [FE_S·$B_{R/S}$] is 75 298 cm^{-1} for [FE_S·B_S] and 75 324 cm^{-1} for [FE_S·B_R]. The complex ions are produced with a strong vibrational excitation of the intramolecular mode of the chromophore, which redistributes very rapidly on the intermolecular modes and dissociates. The higher dissociation ratio found for the heterochiral complex indicates that the order of stability in the ground state is [FE_S·B_S] > [FE_S·B_R].

This observation is confirmed by comparing the 1cR2PI wavelength spectra recorded in correspondence with the

masses of the $[FE_S]^+$ dissociation product and the $[FE_S{\cdot}B_{R/S}]^+$ precursor in the region of the 0^0_0 electronic transition of the two diastereomeric complexes. The spectra in Fig. 5 clearly show a different onset (the arrows in Fig. 5) for the appearance of $[FE_S]^+$ which is located somewhat below 36 867 cm^{-1} for $[FE_S{\cdot}B_R]$ and at about 36 997 cm^{-1} for $[FE_S{\cdot}B_S]$. Therefore the dissociation threshold ($E_{2h\nu}$) of $[FE_S{\cdot}B_R]$ is $<73\,734$ cm^{-1} and that of $[FE_S{\cdot}B_S]$ is about 73 945 cm^{-1}. The difference between the dissociation thresholds of the two $[FE_S{\cdot}B_{R/S}]$ diastereomers corresponds to their binding energy differences in the ground state (ΔD_0). The experimental findings show that the homochiral $[FE_S{\cdot}B_S]$ complex is more stable than the heterochiral $[FE_S{\cdot}B_R]$ complex and that the minimum value of their binding energy difference corresponds to about 210 cm^{-1} (0.60 kcal mol^{-1}). This value compares well with the binding energy differences measured for the non-fluorinated analogues, 1-phenyl-1-propanol/butan-2-ol (1.1 kcal mol^{-1})[13] and 1-phenyl-1-ethanol/butan-2-ol (0.7–1.0 kcal mol^{-1})[14,28] complexes. Also in these systems, the homochiral complexes are more stable than the heterochiral complexes. From the experimental value of ΔD_0 and from the shift of the $S_1 \leftarrow S_0$ transition we can deduce that the homochiral complex is also more stable than the heterochiral complex in the excited state, where the difference in the binding energies is higher by 14 cm^{-1}.

3.3 Theoretical results and structural assignment

Fig. 3 shows the D-B3LYP calculated structures of the most stable ground-state $[FE_S{\cdot}B_R]$ and $[FE_S{\cdot}B_S]$ diastereomers.

In all the most stable complexes the main electrostatic interaction is a hydrogen bond between the alcohol groups of FE_S and $B_{S/R}$ with the solvent acting as a proton acceptor from the OH group of the chromophore and the hydroxyl hydrogen atom of the solvent pointing somewhat towards the aromatic ring plane (OH$\cdots\pi$ bonding). D-B3LYP optimized structures, Fig. 3, predict that the most stable $[FE_S{\cdot}B_{S/R}]$

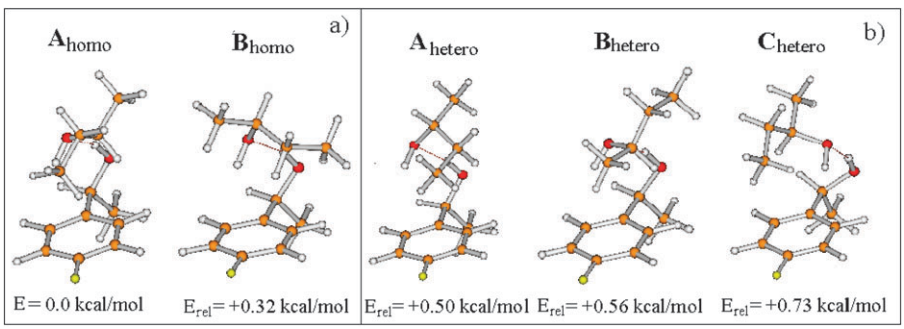

Fig. 3 Structures of the most stable conformers of (a) homochiral $[FE_S{\cdot}B_S]$ and (b) heterochiral $[FE_S{\cdot}B_S]$ complexes and D-B3LYP/6-31G** energies relative to the most stable A_{homo} adduct.

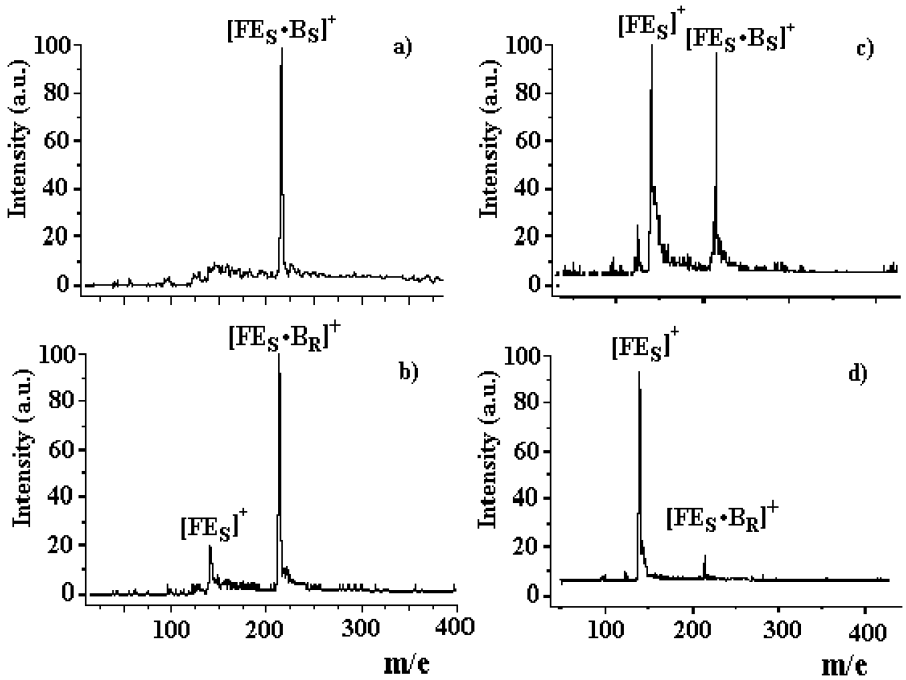

Fig. 4 1cR2PI mass spectra of $[FE_S{\cdot}B_{S/R}]$ clusters taken at: (a) 36 867 cm^{-1} (band 0_0^0 in Fig 1a), (b) 36 853 cm^{-1} (band 0_0^0 in Fig 1a), (c) 37 649 cm^{-1} (band 11 in Fig 1a) and (d) 37 662 cm^{-1} (band 15 in Fig 1b).

structures are characterized by an anti-conformation of the chromophore and an anti C_2–C_3 conformation of the solvent.

The most stable conformer A_{homo} of $[FE_S{\cdot}B_S]$, Fig 3, shows a folded geometry where the methyl group of 2-butanol is bent over the aromatic ring and partially interacts with it. Conformer B_{homo} of $[FE_S{\cdot}B_S]$ is calculated to be less stable than A_{homo} by 0.32 kcal mol^{-1} and differs from A_{homo} by a rotation around the C–O bond and has the alkyl chain of B_S interacting to a minor extent with the aromatic ring. Two quasi-degenerate conformational structures (A_{hetero} and B_{hetero}) are found for $[FE_S{\cdot}B_R]$, differing by only 0.06 kcal mol^{-1} (Fig. 3).

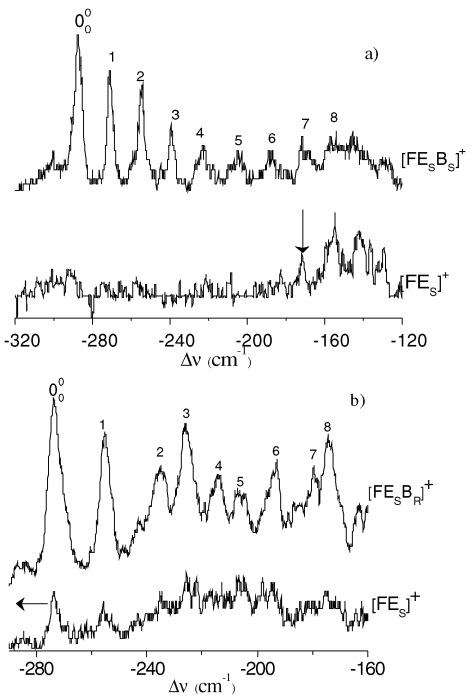

Fig. 5 1cR2PI spectra recorded in correspondence with the mass of the $[FE_S]^+$ dissociation product and the $[FE_S{\cdot}B_{S/R}]^+$ precursors in the region of the 0_0^0 electronic transition of (a) $[FE_S{\cdot}B_S]$ and (b) $[FE_S{\cdot}B_R]$ complexes.

Another conformer C_{hetero} is calculated to be less stable than A_{hetero} by 0.23 kcal mol^{-1}. A_{hetero}, B_{hetero} and C_{hetero} are characterized by a folded geometry where either the methyl (B_{hetero}) or the ethyl (A_{hetero} and C_{hetero}) group of B_R interacts with the aromatic ring. Fig. 3 reports also the energies relative to the most stable A_{homo} adduct. The homochiral complexes have been found to be more stable than the heterochiral complexes, in agreement with the experimental findings. B97D and WB97XD calculations (ESI†) predicted similar conformational structures but, at variance with B3LYP, an higher stability of the heterochiral clusters relative to that of the homochiral clusters was found. Moreover, a better agreement between the experimental and the calculated νO^bH stretching frequencies was found for D-B3LYP than for B97D and WB97XD calculations.

According to D-B3LYP calculations, structure A_{homo} should predominate in the beam. D-B3LYP calculations predict the νO^bH stretching frequency for this conformer at 3635 cm^{-1} in full agreement with the IR-R2PI measured value (Fig. 2a). Therefore, the main feature at 36 853 cm^{-1} in the R2PI spectrum of $[FE_S{\cdot}B_S]$ (Fig. 1a) can be assigned to the corresponding 0_0^0 band origin. D-B3LYP calculations indicate that the low-frequency 17 cm^{-1}-spaced progression of Fig. 1a, starting at 36 853 cm^{-1}, is attributable to the C_1–C_α torsion coupled with intermolecular bending calculated at 23 cm^{-1} for the ground S_0 state of conformer A. In Table 1, the experimental vibronic bands measured for the S_1 excited state are compared with the D-B3LYP calculated vibrational frequencies for the S_0 ground state of the conformer A_{homo}.

IR-R2PI experiments have shown that the two bands 0_0^0 and 3 in the vibronic spectra of $[FE_S{\cdot}B_R]$ (Fig. 1b) are due to the same isomer. The calculated νO^bH stretching frequency of conformer C_{hetero} matches the experimental value much better than that of the A_{hetero} and B_{hetero} isomers (Fig. 2b). We tentatively assign the band at 36 867 cm^{-1} in the spectrum of Fig. 1b to the 0_0^0 origin of the $S_1 \leftarrow S_0$ electronic transition of conformer C_{hetero}, despite its binding energy being lower by 0.23 and 0.17 kcal mol^{-1} than that of the A_{hetero} and B_{hetero} conformers respectively.

Table 2 Experimental vibronic bands of the S_1 excited state of Fig. 1b, compared with the D-B3LYP/6-31G** calculated vibrational frequencies for the S_0 ground state of the C_{hetero} conformer of the $[FE_S{\cdot}B_R]$ cluster

Peak	Vibrational mode	ν_{th}/cm^{-1}	ν_{exp}/cm^{-1}	Mode description
1	ν_1	23	19	C_1–C_α tors. + interm. bend.
2	$2\nu_1$		39	"
3	ν_3	48	47	Interm. tors.
4	$3\nu_1$		60	C_1–C_α torsion + interm. bending
5	$\nu_3 + \nu_1$		67	Interm. torsion + C_1–C_α torsion + interm. bend.
6	ν_4	78	82	Interm. bend.
7	$\nu_3 + 2\nu_1$		87	Interm. tors. + C_1–C_α tors. + interm. bend.
8	$2\nu_3$		94	"
9	$5\nu_1$		100	"
10	ν_6	108	119	C_2–C_3 butanol torsion
11	ν_7	134	138	C_2–C_3 out of pl. bending
12	ν_8	151	151	Interm. bend. + tors. of CH_3 of FE_S
13	ν_9	199	194	C_1–C_α bend.
14	ν_{10}	221	222	Ring out of pl. bend. + butanol CH_3 tors.
15	ν_{32}	784	795	Asym. butterfly
16	$\nu_{32} + \nu_1$		815	Asym. butterfly + C_1–C_α tors. + interm. bend.
17	$\nu_{32} + 2\nu_1$		834	Asym. butterfly + C_1–C_α tors. + interm. bend.
18	ν_{35}	875	891	Methyl bending

The low-frequency, 19 cm^{-1} spaced progression of Fig. 1b, starting at 36 867 cm^{-1}, is attributable to the C_1–C_α torsion coupled with intermolecular bending calculated at 23 cm^{-1} for the ground S_0 state of conformer C_{hetero}. Table 2 compares the experimental vibronic bands measured for the S_1 excited state with the D-B3LYP calculated vibrational frequencies for the S_0 ground state of the conformer C_{hetero}.

The assignment of the spectroscopic data to the structures A_{homo} and C_{hetero} is also supported by the agreement between the D-B3LYP calculated energy difference (0.73 kcal mol^{-1}, Fig. 3) and the experimental value ($\Delta D_0 > 0.60$ kcal mol^{-1}).

4. Conclusions

The present paper presents a spectroscopic investigation on diastereomeric adducts between (*S*)-1-(4-fluorophenyl)-ethanol and *R* and *S* 2-butanol formed in supersonic expansion. The study of the chiral recognition phenomena has been carried out using R2PI spectroscopy with mass selection coupled with infrared-depletion spectroscopy.

The binding energy difference between the homochiral [FE_S·B_S] complex and the heterochiral [FE_S·B_R] diastereomer has been experimentally evaluated to be higher than 0.60 kcal mol^{-1}. This result is in line with previous results on hydrogen bonded complexes between chiral benzylic alcohol derivatives and chiral secondary alcohols. In all the investigated systems, including this study, homochiral complexes were found to be invariably more stable than the heterochiral ones, both in the ground and the excited states. The stability differences in [FE_S·$B_{S/R}$] adducts can be traced to slight structural differences which are reflected by the specific spectroscopic signatures of the $S_1 \leftarrow S_0$ electronic transition as well as different frequencies and intensities of the OH stretch.

In all the most stable [FE_S·$B_{S/R}$] structures, the main electrostatic interaction is a hydrogen bond between the alcohol groups of FE_S and $B_{S/R}$ with the solvent acting as a proton acceptor from the OH group of the chromophore. Both for [FE_S·B_S] and for [FE_S·B_R], one conformation has been observed. They are assigned, on the basis of D-B3LYP calculations, to folded geometries where the methyl (homochiral structure A_{homo}) or the ethyl (heterochiral structure C_{hetero}) group of 2 butanol is bent over the aromatic ring and partially interacts with it.

Acknowledgements

This work was supported by the PRIN grant no. 2007H9S8SW-002 (MIUR). The authors would like to acknowledge Prof. Bernhard Brutschy for his stimulating advice and Massimiliano Lucci, Francesco Toschi and Frédéric Lecomte for their kind help in building the IR-OPO laser.

References

1 (*a*) D. Deamer, S. Singaram, S. Rajamani, V. Kompanichenko and S. Guggenheim, *Philos. Trans. R. Soc. London, Ser. B*, 2006, **361**, 1809–1818; (*b*) A. W. Schwartz, *Curr. Biol.*, 1997, **7**, R477–R499; (*c*) D. Deamer, S. I. Kuzina, A. I. Mikhailov, E. I. Maslikova and S. A. Seleznev, *J. Evol. Biochem. Physiol.*, 1991, **27**, 212–217.
2 (*a*) M. Quack, *Angew. Chem., Int. Ed.*, 2002, **41**, 4618–4630; (*b*) U. J. Meierhenrich and W. H. P. Thiemann, *Origins Life Evol. Biosphere*, 2004, **34**, 111–121; (*c*) D. K. Kondepudi, R. J. Kaufman and N. Singh, *Science*, 1990, **250**, 975–976; (*d*) M. Musigmann, A. Busalla, K. Blum and D. J. Thompson, *J. Phys. B: At., Mol. Opt. Phys.*, 1999, **32**, 4117–4128; (*e*) W. A. Bonner, J. M. Greenberg and E. Rubenstein, *Origins Life Evol. Biosphere*, 1999, **29**, 215–219.
3 R. Popa, *Between Necessity & Probability: Searching for the Definition and Origin of Life*, *Advances in Astrobiology & Biogeophysics Series*, Springer, Berlin Heidelberg, Germany, 2004.
4 K. B. Lipkowitz, S. Raghothama and J. Yang, *J. Am. Chem. Soc.*, 1992, **114**, 1554.
5 L. Pu, *Chem. Rev.*, 2004, **104**, 1687.
6 N. Berova, K. Nakanishi and R. W. Woody, *Circular Dichroism. Principle and Applications*, Wiley, New York, 2000.
7 J. P. Simons, *Mol. Phys.*, 2009, **107**, 2435–2458.
8 A. R. Al Rabaa, E. Breheret, F. Lahmani and A. Zehnacker, *Chem. Phys. Lett.*, 1995, **237**, 480.
9 S. Piccirillo, C. Bosman, D. Toja, A. Giardini, M. Pierini, A. Troiani and M. Speranza, *Angew. Chem., Int. Ed. Engl.*, 1997, **36**, 1729.
10 J. P. Shermann, *Spectroscopy and modelling of biomolecular building blocks*, Elsevier, Amsterdam, 2007, p.341.
11 N. Borho and M. Suhm, *Phys. Chem. Chem. Phys.*, 2002, **4**, 2721.
12 (*a*) A. K. King and B. J. Howard, *Chem. Phys. Lett.*, 2001, **348**, 343; (*b*) Z. Su, N. Borho and Y. Xu, *J. Am. Chem. Soc.*, 2006, **128**, 17126.
13 M. Speranza, M. Satta, S. Piccirillo, F. Rondino, A. Paladini, A. Giardini, A. Filippi and D. Catone, *Mass Spectrom. Rev.*, 2005, **24**, 588–610.
14 M. Mons, F. Piuzzi, I. Dimicoli, A. Zehnacker and F. Lahmani, *Phys. Chem. Chem. Phys.*, 2000, **2**, 5065–5070.
15 A. Giardini, F. Rondino, A. Paladini, M. Speranza, M. Satta and S. Piccirillo, *J. Phys. Chem. A*, 2009, **113**(52), 15127–15135.
16 M. Speranza, F. Rondino, A. Giardini, A. Paladini, A. R. Hortal, S. Piccirillo and M. Satta, *ChemPhysChem*, 2009, **10**, 1859.
17 (*a*) K. L. Kirk, *J. Fluorine Chem.*, 2006, **127**, 1013–1029; (*b*) C. Isanbor and D. O'Hagan, *J. Fluorine Chem.*, 2006, **127**, 303–319; (*c*) J. P. Bégué and D. Bonnet-Delpon, *J. Fluorine Chem.*, 2006, **127**, 992–1012.
18 S. Piccirillo, M. Coreno, A. Giardini-Guidoni, G. Pizzela, M. Snels and R. Teghil, *J. Mol. Struct.*, 1993, **293**, 197.
19 E. G. Robertson and J. P. Simons, *Phys. Chem. Chem. Phys.*, 2001, **3**, 1–18.
20 B. Reimann, K. Buchhold, H. D. Barth, B. Brutschy, P. Tarakeshwar and K. S. Kim, *J. Chem. Phys.*, 2002, **117**, 1.
21 P. Ren and J. W. Ponder, *J. Phys. Chem. B*, 2003, **107**, 5933–5947.
22 N. L. Allinger, Y. H. Yuh and J. H. Lii, *J. Am. Chem. Soc.*, 1989, **111**, 8551.
23 S. Grimme, *J. Comput. Chem.*, 2004, **25**, 1463.
24 M. W. Wong, *Chem. Phys. Lett.*, 1996, **256**, 391.
25 M. J. Frisch, G. W. Trucks, H. B. Schlegel, G. E. Scuseria, M. A. Robb, J. R. Cheeseman, V. G. Zakrzewski, J. A. Montgomery, R. E. Stratmann, J. C. Burant, S. Dapprich, J. M. Millam, A. D. Daniels, K. N. Kudin, M. C. Strain, O. Farkas, J. Tomasi, V. Barone, M. Cossi, R. Cammi, B. Mennucci, C. Pomelli, C. Adamo, S. Clifford, J. Ochterski, G. A. Petersson, P. Y. Ayala, Q. Cui, K. Morokuma, D. K. Malick, A. D. Rabuck, K. Raghavachari, J. B. Foresman, J. Cioslowski, J. V. Ortiz, A. G. Baboul, B. B. Stefanov, G. Liu, A. Liashenko, P. Piskorz, I. Komaromi, R. Gomperts, R. L. Martin, D. J. Fox, T. Keith, M. A. Al-Laham, C. Y. Peng, A. Nanayakkara, M. Challacombe, P. M. W. Gill, B. G. Johnson, W. Chen, M. W. Wong, J. L. Andres, C. Gonzalez, M. Head-Gordon, E. S. Replogle and J. A. Pople, *Gaussian 03*, Gaussian, Inc., Pittsburgh, PA, 2003.
26 High Performance Computational Chemistry Group, NWChem, A Computational Chemistry Package for Parallel Computers, Version 5.0.1 (2001), Pacific Northwest National Laboratory, Richland, Washington 99352, USA.
27 M. W. Schmidt, K. K. Baldridge, J. A. Boatz, S. T. Elbert, M. S. Gordon, J. H. Jensen, S. Koseki, N. Matsunaga, K. A. Nguyen, S. J. Su, T. L. Windus, M. Dupuis and J. A. Montgomery, *J. Comput. Chem.*, 1993, **14**, 1347.
28 A. Giardini-Guidoni, S. Piccirillo, D. Scuderi, M. Satta, T. M. Di Palma, M. Speranza, A. Filippo and A. Paladini, *Chirality*, 2001, **13**, 727–730.
29 K. Le Barbu, A. Zehnacker, F. Lahmani, M. Mons, F. Piuzzi and I. Dimicoli, *Chirality*, 2001, **13**, 715–721.
30 B. Brutschy, *J. Phys. Chem.*, 1990, **94**, 8637–8647.

